

Lawrence Berkeley National Laboratory

Lawrence Berkeley National Laboratory

Title

Microwave Plasma Chemical Vapor Deposition of Carbon Coatings on $\text{LiNi}_{1/3}\text{Co}_{1/3}\text{Mn}_{1/3}\text{O}_2$ for Li-Ion Battery Composite Cathodes

Permalink

<https://escholarship.org/uc/item/9x08q2dp>

Author

Doeff, M.M.

Publication Date

2009-04-15

**Microwave Plasma Chemical Vapor Deposition of Carbon Coatings on
LiNi_{1/3}Co_{1/3}Mn_{1/3}O₂ for Li-ion Battery Composite Cathodes**

Marek L. Marcinek^{ab}, James W. Wilcox^b, Marca M. Doeff^{bc} and Robert M. Kostecki^{*b}

Environmental Energy Technologies Division

^cMaterials Sciences Division

Lawrence Berkeley National Laboratory

University of California

Berkeley, CA 94720, USA

Abstract

In this paper, we report results of a novel synthesis method of thin film conductive carbon coatings on LiNi_{1/3}Co_{1/3}Mn_{1/3}O₂ cathode active material powders for lithium-ion batteries. Thin layers of graphitic carbon were produced from a solid organic precursor, anthracene, by a one-step microwave plasma chemical vapor deposition (MPCVD) method. The structure and morphology of the carbon coatings were examined using SEM, TEM, and Raman spectroscopy. The composite LiNi_{1/3}Co_{1/3}Mn_{1/3}O₂ electrodes were electrochemically tested in lithium half coin cells. The composite cathodes made of the carbon-coated LiNi_{1/3}Co_{1/3}Mn_{1/3}O₂/C powder showed superior electrochemical performance and increased capacity compared to standard composite LiNi_{1/3}Co_{1/3}Mn_{1/3}O₂ electrodes.

^a Current address: The Warsaw University of Technology, Warsaw, Poland.

^b Electrochemical Society Active Member

*Corresponding author.

E-mail address: r_kostecki@lbl.gov, tel: 00 1 510 486 6002, fax: 00 1 510 486 7303

Introduction

The new generation of layered mixed transition metal oxides, LiMO_2 ($\text{M}=\text{Co}$, Ni , and Mn), with the $\alpha\text{-NaFeO}_2$ structure currently considered for use as cathode materials in Li-ion batteries offers a high, reversible charge capacity and improved safety performance. These compounds, which include $\text{LiNi}_{1/3}\text{Co}_{1/3}\text{Mn}_{1/3}\text{O}_2$ (LNCMO) among other compositions, are potential candidates to replace commercial LiCoO_2 . $\text{LiNi}_{1/3}\text{Co}_{1/3}\text{Mn}_{1/3}\text{O}_2$ exhibits reversible capacities of $\sim 200 \text{ mAhg}^{-1}$ between 2.8–4.6 V and $\sim 160 \text{ mAhg}^{-1}$ between 2.5–4.4 V [1,2,3,4]. The electrochemical processes below $\sim 4.3\text{V}$ primarily involve the two electron transfers $\text{Ni}^{2+} \leftrightarrow \text{Ni}^{4+}$, whereas the oxidation state of Co and Mn ions remains +2 and +4, respectively [5].

Low electronic conductivity of cathode active materials can limit the power capability of lithium batteries. Conductive carbon additives are routinely used to enhance the utilization of the active material in composite cathodes and improve rate performance. This problem is acutely pronounced for olivine-structured LiMPO_4 materials ($\text{M}=\text{Fe}$, Mn), which exhibit inherently low electronic conductivity ($<10^{-9} \text{ Scm}^{-1}$ for LiFePO_4) [6,7]. To overcome the insulating behavior of the phosphate, the particles are often coated with a thin, conductive layer of pyrolytic carbon from various organic precursors [8,9,10,11,12,13]. The conductivity percolation threshold for C-coated nano-structured phosphate particles is usually observed at $\sim 1.5 \text{ wt. \%}$ of carbon [12,13].

The oxide-based cathode materials exhibit much higher electronic conductivity ($10^{-1}\text{-}10^{-5} \text{ Scm}^{-1}$) [14,15]. The composite oxide cathodes consist of a simple mechanical

mixture of active material, conductive carbon additive, and binder. However, such a simple manufacturing procedure can produce quite a non-uniform distribution of carbon black in the composite electrode [16] that may lead to non-uniform utilization of the active material and loss of reversible charge capacity and rate capability [17].

The effect of coating oxide-based cathode materials with conductive carbon layers has been investigated less often than that of carbon-coated olivines. Direct carbon-black coating of oxide cathode materials using a gelatin surfactant helped improve the carbon distribution, and consequently, increased the capacity of a Li-ion cell and minimized cell polarization [16,18]. The pyrolyzed carbon coating from a resorcinol-formaldehyde polymer on $\text{LiMn}_{0.5}\text{Ni}_{0.5}\text{O}_2$ [19] or acrylonitrile and styrene-acrylonitrile-based polymers on LiMn_2O_4 spinel [20] suppressed capacity fade and reduced cell polarization. The amorphous carbon coating from pyrolyzed sugar on $\text{LiNi}_{1/3}\text{Mn}_{1/3}\text{Co}_{1/3}\text{O}_2$ improved thermal stability and rate capability of the cathode [21].

LNCMO materials are most commonly synthesized by a mixed hydroxide method and calcined in air or in pure oxygen at temperatures >800 °C. Under these conditions, carbon formed from any added organic precursors either during synthesis or in a post-treatment step is likely to oxidize to CO. Furthermore, carbothermal reduction to the elemental metals or reduced oxides may occur if the reaction is carried out under an inert atmosphere to prevent loss of carbon[19,21]. At low temperatures, highly amorphous carbons of poor and highly non-uniform electronic conductivity are formed [22]. Thus it is not straightforward to co-synthesize LNCMO/C composites as is typically done with

LiFePO₄/C.

High-power microwave plasma chemical vapor deposition (MPVCD) techniques have been widely used to prepare thin-films of diamond [23,24] and carbon nano-tubes [25,26]. The MPVCD synthesis of amorphous, sp²- coordinated carbon thin-films [27], carbon fibers [28], and nano-crystalline graphite (NCG) [29] has also been published. Recent reports on MPVCD synthesis of carbon-Pt and carbon-Sn composite thin films [30,31] for fuel cell and battery applications demonstrate the potential of this experimental approach. The objective of this work was to adapt and use MPCVD to produce highly conductive graphitic coatings on cathode active material powders and enhance their electrochemical performance in Li-ion batteries [32].

Experimental

Figure 1 shows a diagram of the two-segment Pyrex glass tube and a schematic representation of the deposition process. Carbonaceous films can be produced on various types of conductive and non-conductive substrate materials from organic precursor without using stabilizers or reducing agents. A detailed description of the experimental setup can be found in [30,31]. In this work, a small amount (~2 mg) of anthracene (Sigma–Aldrich) organic precursor was placed at one end of a glass slide and ~200 mg of LiNi_{1/3}Co_{1/3}Mn_{1/3}O₂ powder (SEIMI) was positioned ~5 mm away from the precursor at the other end of the glass slide. The reactor was purged with Ar for 30s with a flow of 3 dm³/min, evacuated to 1.1x10⁻¹ Torr, and positioned in close vicinity to a 2.45 GHz, 1200 W magnetron. The MPACVD reactor was enclosed in a nitrogen-filled glove box to

eliminate any possible interference from oxygen impurities.

The Ar-plasma discharge resulted in a fast evaporation of the anthracene precursor followed by a rapid pyrolysis and precipitation of carbon on the $\text{LiNi}_{1/3}\text{Co}_{1/3}\text{Mn}_{1/3}\text{O}_2$ powder. The geometry of the system was designed to keep the hot edge of the Ar-plasma near the organic precursor source and the cool edge of the plasma glow near the substrate. A typical MPCVD process was carried out at 1200 W microwave radiation power for 2s and produced ~10-20 nm thick carbon layer on the powder. The deposition process was repeated three times for each powder sample. To ensure a relatively uniform carbon coating, the $\text{LiNi}_{1/3}\text{Co}_{1/3}\text{Mn}_{1/3}\text{O}_2$ powder sample was agitated prior to each deposition. The qualitative analysis of the carbon coated powders by inductively coupled plasma spectroscopy and combustion infrared detection produced a carbon content of 0.8-1.2 % wt.

The structure of carbon in composite Sn/C films was analyzed by Raman microscopy (Labram, ISA Group Horiba) with a laser excitation wavelength of 632.8 nm, at 1 mW power at the sample surface. The morphology of the $\text{LiNi}_{1/3}\text{Co}_{1/3}\text{Mn}_{1/3}\text{O}_2$ powder and the thin-film coating were characterized by transmission electron microscopy (TEM, model JEOL 200CX), and scanning electron microscopy (SEM, model Hitachi S-4300 SE/N). An X-ray powder diffraction pattern of a $\text{LiNi}_{1/3}\text{Co}_{1/3}\text{Mn}_{1/3}\text{O}_2$ /C material was obtained using a Philips X-Pert PRO diffractometer operating in Bragg-Brentano mode with $\text{Cu K}\alpha$ radiation.

LiNi_{1/3}Co_{1/3}Mn_{1/3}O₂ composite electrodes were prepared as follows. The composite thin-film (~60 μm, ~1 mAhcm⁻²) cathodes consisted of a 84 wt.% of pure LiNi_{1/3}Co_{1/3}Mn_{1/3}O₂ or carbon-coated LiNi_{1/3}Co_{1/3}Mn_{1/3}O₂/C, 4 wt.% carbon black (Shawinigan), 4 wt.% SFG-6 (TIMCAL), and 8 wt.% PVdF (Kureha) deposited from a 1-methyl-2-pyrrolidinone slurry on carbon-coated Al foil (Intelicoat Technologies). The freshly prepared electrodes were dried in a He-filled glove box antechamber vacuum oven at 120 °C, 0.2 Torr for 42 h. Disks of 1.8 cm² were punched from the cast electrode and assembled in 2032 coin cells with Li-foil anodes, Celgard 3401 separators, and 1 M LiPF₆, ethylene carbonate + dimethylcarbonate (EC/DMC, 1:2wt.%) electrolyte solutions in an inert atmosphere glovebox.

Electrochemical characterization was conducted at room temperature using a BT/HSP-2043 (Arbin Instruments) testing system. The coin cells were cycled galvanostatically between 2.0 and 4.4 V. The charge process was always carried out at C/25 rate followed by a 15 min relaxation period at an open circuit voltage, unless otherwise specified.

Results and Discussion

Fig. 2 shows the X-ray diffraction patterns of the original LiNi_{1/3}Co_{1/3}Mn_{1/3}O₂ and MPCVD carbon-coated LiNi_{1/3}Co_{1/3}Mn_{1/3}O₂/C powders. All peaks could be indexed to space group *R3_m* (the α-NaFeO₂ structure), in both cases. The pattern of LiNi_{1/3}Co_{1/3}Mn_{1/3}O₂/C is nearly identical to pure LiNi_{1/3}Co_{1/3}Mn_{1/3}O₂ indicating that no thermal decomposition or phase transformation (including formation of a superlattice

structure caused by rearrangement of metal ions in $3a$ sites) took place during the microwave treatment. No peaks attributable to graphite could be detected in the pattern of $\text{LiNi}_{1/3}\text{Co}_{1/3}\text{Mn}_{1/3}\text{O}_2/\text{C}$ due to its low carbon content.

The typical Raman spectra of fresh $\text{LiNi}_{1/3}\text{Co}_{1/3}\text{Mn}_{1/3}\text{O}_2$ and MPCVD carbon-coated $\text{LiNi}_{1/3}\text{Co}_{1/3}\text{Mn}_{1/3}\text{O}_2/\text{C}$ powders recorded at 632.8 nm excitation wavelength are displayed in Fig. 3. The Raman active vibrations that correspond to the M–O stretching and O–M–O bending modes within MO_2 layers are generally contained between 400 and 650 cm^{-1} [33,34,35]. The group centered at $\sim 590\text{ cm}^{-1}$ (Fig. 3a and b) is comprised of bands at 474, 554 (Ni–O), 594 cm^{-1} (Mn–O), and 486, 596 cm^{-1} (Co–O) that represent the vibrations within the hexagonal MO_2 lattice.

The spectrum of $\text{LiNi}_{1/3}\text{Co}_{1/3}\text{Mn}_{1/3}\text{O}_2/\text{C}$ (Fig. 3b) exhibits two intense peaks assigned as the G- and D-band at 1596 and 1325 cm^{-1} that correspond to the E_{2g} and A_{1g} carbon vibration modes, respectively [36]. The D-band is associated with the break in symmetry that occurs at the edges of the graphite sheets. A shoulder at 1620 cm^{-1} , known as the D'-band, is also attributed to discontinuity and disorder within graphene planes, but the exact nature of this peak is still under dispute [37].

The presence of strong graphite G and D modes along with the absence of a sharp diamond Raman peak at $\sim 1330\text{ cm}^{-1}$ in the Raman spectra suggests that the carbon film consists of a sp^2 -coordinated carbon phase similar to nano-crystalline graphite with a high degree of disorder [38]. The presence of Raman bands characteristic of

$\text{LiNi}_{1/3}\text{Co}_{1/3}\text{Mn}_{1/3}\text{O}_2$ in the spectrum of the carbon-coated material indicates that the carbon layer is relatively thin and/or non-uniform. Importantly, the Raman spectra of the $\text{LiNi}_{1/3}\text{Co}_{1/3}\text{Mn}_{1/3}\text{O}_2/\text{C}$ composite powder corroborate the XRD data in that there is no sign of new phase formation due to, e.g., thermal decomposition.

SEM images of the fresh and carbon-coated powders are shown in Fig. 4. The $\text{LiNi}_{1/3}\text{Co}_{1/3}\text{Mn}_{1/3}\text{O}_2$ powder constitutes of $0.5 \times 2 \mu\text{m}$ elongated primary particles fused tightly into large $8\text{-}10 \mu\text{m}$ polycrystalline spherical agglomerates. Interestingly, the carbon layer cannot be clearly identified in the micrograph of $\text{LiNi}_{1/3}\text{Co}_{1/3}\text{Mn}_{1/3}\text{O}_2/\text{C}$ due to its inherent thinness. The SEM images show no visible structural or morphology changes in the $\text{LiNi}_{1/3}\text{Co}_{1/3}\text{Mn}_{1/3}\text{O}_2$ oxide particles that could result from overheating or chemical reactions with the carbon film.

The HRTEM image of the carbon-coated $\text{LiNi}_{1/3}\text{Co}_{1/3}\text{Mn}_{1/3}\text{O}_2/\text{C}$ (Fig. 5) reveals an ca. 10 nm thick layer of carbonaceous material with an average interlayer spacing $d_{002}=3.6 \text{ \AA}$. The large d-spacing compared to that of graphite (3.3545 \AA) is typical for carbon blacks where graphene planes are parallel but randomly shifted with no turbostratic order. On the other hand, the relatively large dimensions $\sim 30\text{-}50 \text{ \AA}$ of graphene clusters in the carbon film correspond to graphitized carbon blacks produced by heat treatment at $T > 1500^\circ\text{C}$. The carbon layer also displays regions where shorter layers of irregular shape prevail, which are typical of carbon blacks [39].

To evaluate the power capability of the carbon-coated $\text{LiNi}_{1/3}\text{Co}_{1/3}\text{Mn}_{1/3}\text{O}_2/\text{C}$ material, the composite electrode was tested at different discharge rates. Figure 6 shows the discharge curves for the carbon coated and uncoated powders at $C/2$, $1C$, and $2C$ rates, which correspond to 0.5, 1.0, and 2.0 mA/cm^2 discharge currents, respectively. The rate performance of the $\text{LiNi}_{1/3}\text{Co}_{1/3}\text{Mn}_{1/3}\text{O}_2/\text{C}$ composite cathode exhibits a smaller polarization potential drop and better capacity retention than the electrode produced with the uncoated $\text{LiNi}_{1/3}\text{Co}_{1/3}\text{Mn}_{1/3}\text{O}_2$ powder. Such improved rate performance suggests that the thin graphite layer on active material particles helps assure good electronic contact within the composite cathode and does not impede Li^+ transport across the $\text{LiNi}_{1/3}\text{Co}_{1/3}\text{Mn}_{1/3}\text{O}_2/\text{electrolyte}$ interface.

The cycling performance of the uncoated and carbon-coated $\text{LiNi}_{1/3}\text{Co}_{1/3}\text{Mn}_{1/3}\text{O}_2/\text{C}$ composite cathodes is illustrated in Figure 7. The galvanostatic charge-discharge cycling of the carbon-coated $\text{LiNi}_{1/3}\text{Co}_{1/3}\text{Mn}_{1/3}\text{O}_2/\text{C}$ electrode over 40 cycles at $C/5$ rate shows only $\sim 4\%$ capacity fading, which presents a significant improvement compared to the electrochemical performance of the uncoated electrode, which displays $\sim 10\%$ capacity fade at the end of cycling.

The improved electrochemical behavior of the MPCVD C-coated $\text{LiNi}_{1/3}\text{Co}_{1/3}\text{Mn}_{1/3}\text{O}_2$ material is due to better electrical contact between the particles in the composite cathode as well as the current collector. In the absence of any significant structural degradation, the capacity loss and cell impedance rise are usually associated with the loss of electronic conductivity within the composite cathode [35]. It is

particularly important to provide a direct conductivity path to the primary particles in larger agglomerates of active material, which are often intrinsically in poor electronic contact with each other [40]. The slightly higher carbon content in the composite electrode manufactured from the carbon-coated $\text{LiNi}_{1/3}\text{Co}_{1/3}\text{Mn}_{1/3}\text{O}_2/\text{C}$ could have also contributed to the improvement the electrochemical performance. However, it has been demonstrated that the uniformity of carbon additive distribution within the composite electrode is a critical parameter that determines the electrode kinetics [16].

A simple co-synthesis or pyrolytic route to produce carbon coatings is not available in this case because the oxides are usually synthesized in air or under oxygen at temperatures $>800\text{ }^\circ\text{C}$, which will oxidize any carbon source to CO_2 or CO . The MPCVD of thin graphitized carbon coatings on lithium metal oxides offers a unique and effective way of enhancing the rate and cycling performance of metal oxide cathode materials for Li-ion batteries. This manufacturing methodology provides an easy, fast, and inexpensive method for the direct formation of uniform and highly conductive carbon thin films on any type of electrode materials. Although the present batch process is impractical for large scale production, MPCVD can be easily envisioned in a continuous deposition configuration which allows nonstop feeding of electrode material into the reactor.

Conclusions

We demonstrated a novel direct deposition method of thin film conductive graphitized carbon coatings on $\text{LiNi}_{1/3}\text{Co}_{1/3}\text{Mn}_{1/3}\text{O}_2$ cathode active material powder for lithium-ion batteries. Thin layers of graphitic carbon were produced from a solid organic

precursor anthracene by a one step microwave plasma chemical vapor deposition (MPCVD). The carbon deposition process did not induce thermal decomposition or transformation to new oxide phases. The carbon film consists of a sp^2 -coordinated carbon phase similar to nano-crystalline graphite with a high degree of disorder, which corresponds to graphitized carbon blacks produced otherwise by pyrolysis at $T > 1500^\circ\text{C}$. The improved electrochemical behavior of the MPCVD C-coated $\text{LiNi}_{1/3}\text{Co}_{1/3}\text{Mn}_{1/3}\text{O}_2$ material is due to good electrical contact between primary particles of the active material. The thin graphite layer on active material particles helps assure good electronic contact within the composite cathode and does not impede Li^+ transport across the $\text{LiNi}_{1/3}\text{Co}_{1/3}\text{Mn}_{1/3}\text{O}_2/\text{electrolyte}$ interface.

Acknowledgment

This work was supported by the Assistant Secretary for Energy Efficiency and Renewable Energy, Office of FreedomCAR and Vehicle Technologies of the U.S. Department of Energy under Contract No. DE-AC02-05CH11231.

References

1. T. Ohzuku, Y. Makimura, *Chem. Lett.* **7** (2001) 642
2. K.M. Shaju, G.V. Subba Rao, B.V.R. Chowdari, *Electrochim. Acta*, **48** (2002) 145
3. N. Yabuuchi, T. Ohzuku, *J. Power Sources*, **119–121** (2003), 171
4. K. M. Shaju, G. V. Subba Rao, B. V. R. Chowdari, *J. Electrochem. Soc.*, **151** (2004) A1324

5. B.J. Hwang, Y.W. Tsai, D. Cariler, G. Ceder, *Chem. Mater.*, 15 (2003) 376
6. A.K. Pahdi, K.S. Nanjundaswamy, J.B. Goodenough, *J. Electrochem. Soc.*, 144 (1997) 1188
7. J. Chen, M.J. Vacchio, S. Wang, N. Chernova, P.Y. Zavalij, M.S. Whittingham, *Solid State Ionics*, 178 (2008) 1676, and references therein
8. N. Ravet, J.B. Goodenough, S. Besner, M. Simoneau, P. Hovington, M. Armand, *Electrochem. Soc. Abstracts 99-2* (1999) 127.
9. N. Ravet, S. Besner, M. Simoneau, A. Vallée, M. Armand, J.-F. Magnan, Hydro-Quebec, European Patent (2000) 1049182A2
10. N. Ravet, Y. Chouinard, J.F. Magnan, S. Besner, M. Gauthier, M. Armand, J. *Power Sources 97-98* (2001) 503
11. H. Huang, S.-C. Yin, L.F. Nazar, *Electrochem. Solid-State Lett.*, 4 (2001) A170
12. J.D. Wilcox, M.M. Doeff, M. Marcinek, R. Kostecki, *J. Electrochem. Soc.*, 154 (2007) A389
13. R. Dominko, J.M. Goupil, M. Bele, M. Gaberšček, M. Remskar, D. Hanzel, J. Jamnik, *J. Electrochem. Soc.*, 152 (2005) A607
14. J. Molenda, K. Swierczek, W. Kucza, J. Marzec, A. Stoklosa, *Solid State Ionics* 123 (1999) 155
15. J. Xie, N. Imanishi, T. Matsumura, A. Hirano, Y. Takeda, O. Yamamoto, *Solid State Ionics* 179 (2008) 362
16. R. Dominko, M. Gaberšček, J. Drofenik, M. Bele, J. Jamnik, *Electrochim. Acta*, 48 (2003) 3709
17. Jinglei Lei, Frank McLarnon, Robert Kostecki, *J. Phys. Chem. B*, 109 (2005) 952

18. J. Kim, B. Kim, J.-G Lee, J. Cho, B. Park, *J. Power Sources*, 139 (2005) 289
19. B.L. Cushing, J.B. Goodenough, *Solid State Sciences*, 4 (2002) 1487
20. M. Molenda, R. Dziembaj, E. Podstawka, L.M. Proniewicz, Z. Piwowarska, *J. Power Sources*, 174 (2007) 613
21. H.-S. Kim, M. Kong, K. Kim, I.-J. Kim, H.-B. Gub, *J. Power Sources*, 171 (2007) 917
22. R. Kostecki, B. Schnyder, D. Alliata, X. Song, K. Kinoshita, R. Kötz, *Thin Solid Films* 396 (2001) 36
23. V.G. Ralchenko, A.A. Smolin, V.I. Konov, K.F. Sergeichev, I.A. Sychov, I.I. Vlasov, V.V. Migulin, S.V. Voronina, A.V. Khomich, *Diamond Relat. Mater.* 6 (1997) 417
24. T.P. Mollart, K.L. Lewis, *Diamond Relat. Mater.* 8 (1999) 236
25. O.M. Kuttel, O. Groening, L. Schlapbach, *Appl. Phys. Lett.* 73 (1998) 2113
26. H. Murakami, M. Hirakawa, C. Tanaka, H. Yamakawa, *Appl. Phys. Lett.* 76 (2000) 1776
27. Y. Lifshitz, C.H. Lee, Y. Wu, W.J. Zhang, I. Bello, S.T. Lee, *Appl. Phys. Lett.* 88 (2006) 243114
28. J. Zou, X. Zeng, X. Xiong, H. Tang, L. Li, Q. Liu, Z. Li, *Carbon* 45 (2007) 828
29. R.C. Mani, M.K. Sunkara, R.P. Baldwin, J. Gullapalli, J.A. Chaney, G. Bhimarasetti, J.M. Cowley, A.M. Rao, R. Raod, *J. Electrochem. Soc.* 152 (2005) E154.
30. M. Marcinek, X. Song, R. Kostecki, *Electrochem. Commun.*, 9 (2007) 1739

31. M. Marcinek, L.J. Hardwick, T.J. Richardson, X. Song, R. Kostecki, *J. Power Sources*, 173 (2007) 965
32. M. Marcinek, R. Kostecki, in: 208th Electrochem. Soc. Meeting, Los Angeles, October 16–21, 2005, Abstract #114
33. C. Julien, *Solid State Ionics* 136/137 (2000) 887
34. C. Julien, *Solid State Ionics* 157 (2000) 57
35. M. Kerlau, M. Marcinek, V. Srinivasan, R. Kostecki, *Electrochimica Acta* 52 (2007) 5422
36. F. Tunistra and J.L. Koenig, *J. Chem. Phys.* 53 (1970), 1126
37. M.A. Pimenta, G. Dresselhaus, M.S. Dresselhaus, L.G. Cancado, A. Jorio, R. Saito, *Phys. Chem. Chem. Phys.* 9 (2007) 1276
38. A.D. Lueking, H.R. Gutierrez, D.A. Fonseca, E. Dickey, *Carbon* 45 (2007) 751, and references therein.
39. K. Kinoshita, “Carbon, Electrochemical and Physicochemical Properties”, 1988 by John Willey & Sons, Inc., and references therein.
40. R. Kostecki, F. McLarnon, *Electrochem. Solid State Lett.* 7 (2004) A380

Figure Captions

Figure 1. A diagram of the microwave plasma chemical vapor deposition system (a), schematic representation of the deposition of carbon thin-films on $\text{LiNi}_{1/3}\text{Co}_{1/3}\text{Mn}_{1/3}\text{O}_2$ powder (b).

Figure 2. X-ray diffraction pattern of the fresh $\text{LiNi}_{1/3}\text{Co}_{1/3}\text{Mn}_{1/3}\text{O}_2$ and MPCVD coated $\text{LiNi}_{1/3}\text{Co}_{1/3}\text{Mn}_{1/3}\text{O}_2/\text{C}$ powders.

Figure 3. Micro-Raman spectra of the fresh $\text{LiNi}_{1/3}\text{Co}_{1/3}\text{Mn}_{1/3}\text{O}_2$ (a) and $\text{LiNi}_{1/3}\text{Co}_{1/3}\text{Mn}_{1/3}\text{O}_2/\text{C}$ (b) powders recorded at 632.8 nm excitation wavelength.

Figure 4. SEM micrographs of the fresh $\text{LiNi}_{1/3}\text{Co}_{1/3}\text{Mn}_{1/3}\text{O}_2$ (a) and MPCVD $\text{LiNi}_{1/3}\text{Co}_{1/3}\text{Mn}_{1/3}\text{O}_2/\text{C}$ (b) powders.

Figure 5. HRTEM image of the MPCVD carbon-coated $\text{LiNi}_{1/3}\text{Co}_{1/3}\text{Mn}_{1/3}\text{O}_2/\text{C}$ powder.

Figure 6. Discharge capacities of Li cells containing $\text{LiNi}_{1/3}\text{Co}_{1/3}\text{Mn}_{1/3}\text{O}_2$ (solid line) and $\text{LiNi}_{1/3}\text{Co}_{1/3}\text{Mn}_{1/3}\text{O}_2/\text{C}$ (dashed line) cathodes at different rates (cells were charged at C/25 prior to discharge at given rate).

Figure 7. Discharge capacities of Li cells containing $\text{LiNi}_{1/3}\text{Co}_{1/3}\text{Mn}_{1/3}\text{O}_2$ (●), and $\text{LiNi}_{1/3}\text{Co}_{1/3}\text{Mn}_{1/3}\text{O}_2/\text{C}$ (▼) cathodes during cycling at room temperature at C/5 rate between 4.3 and 2.0V. (charging was carried out at C/25 rate).

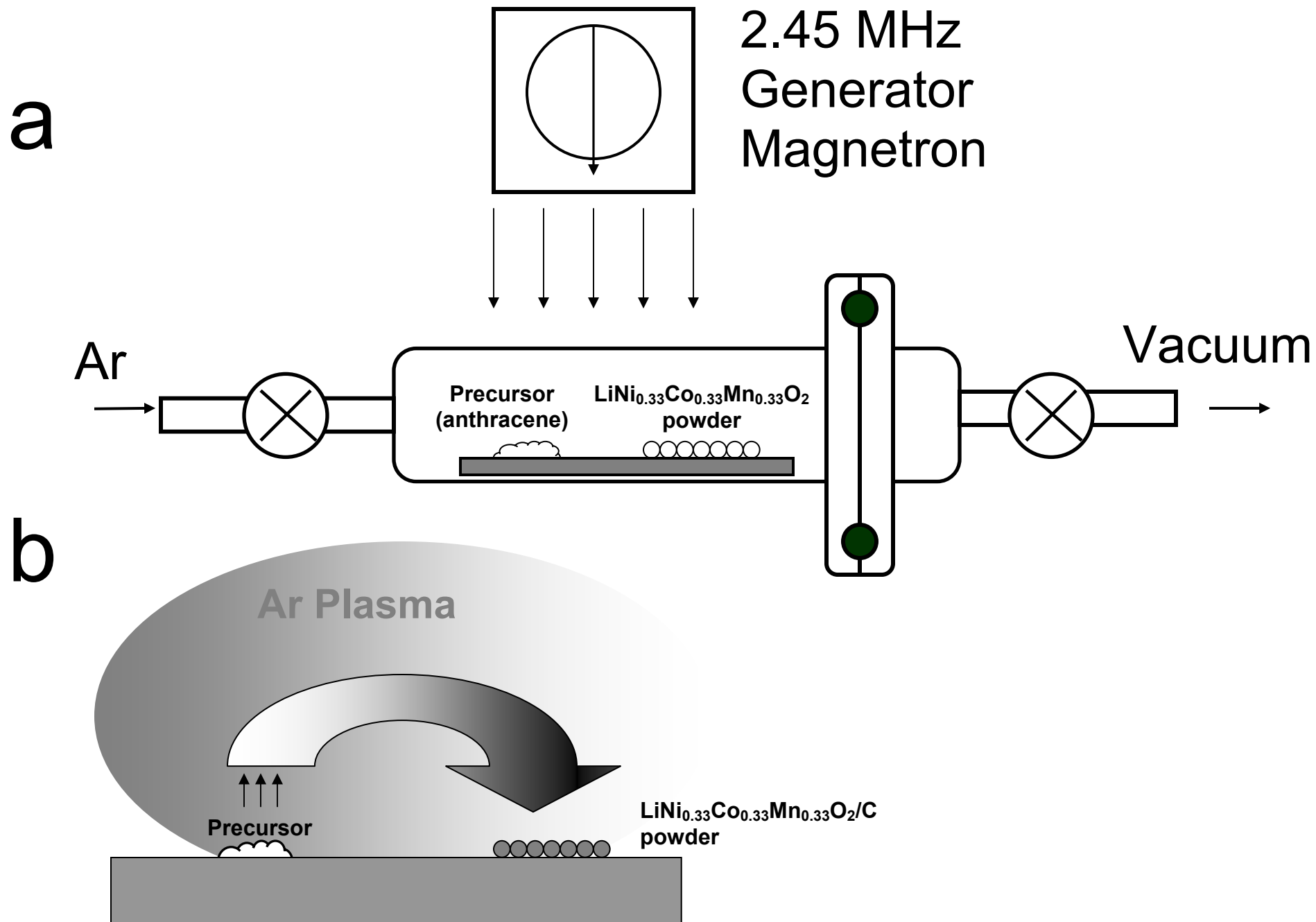


Figure 1

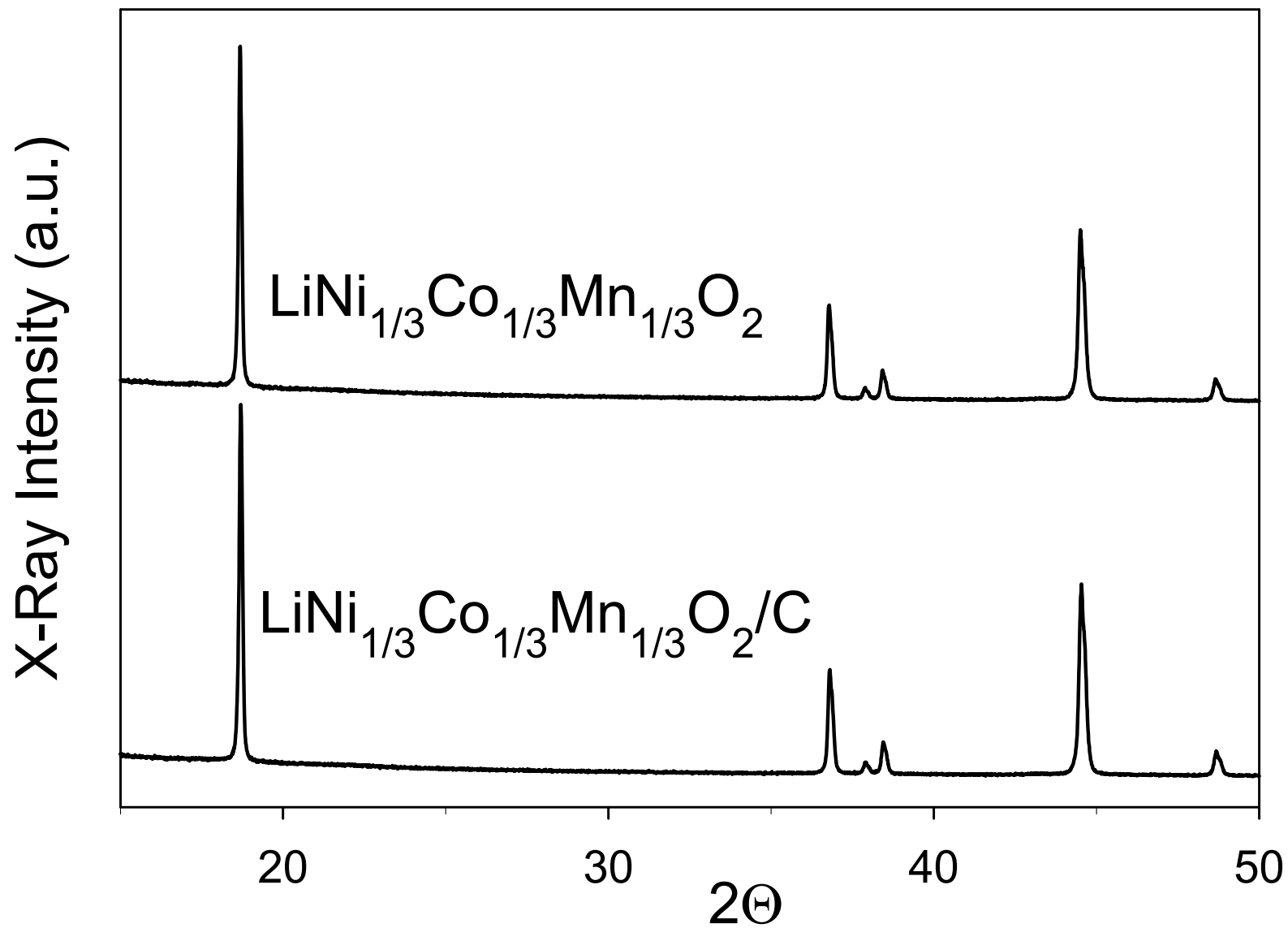


Figure 2

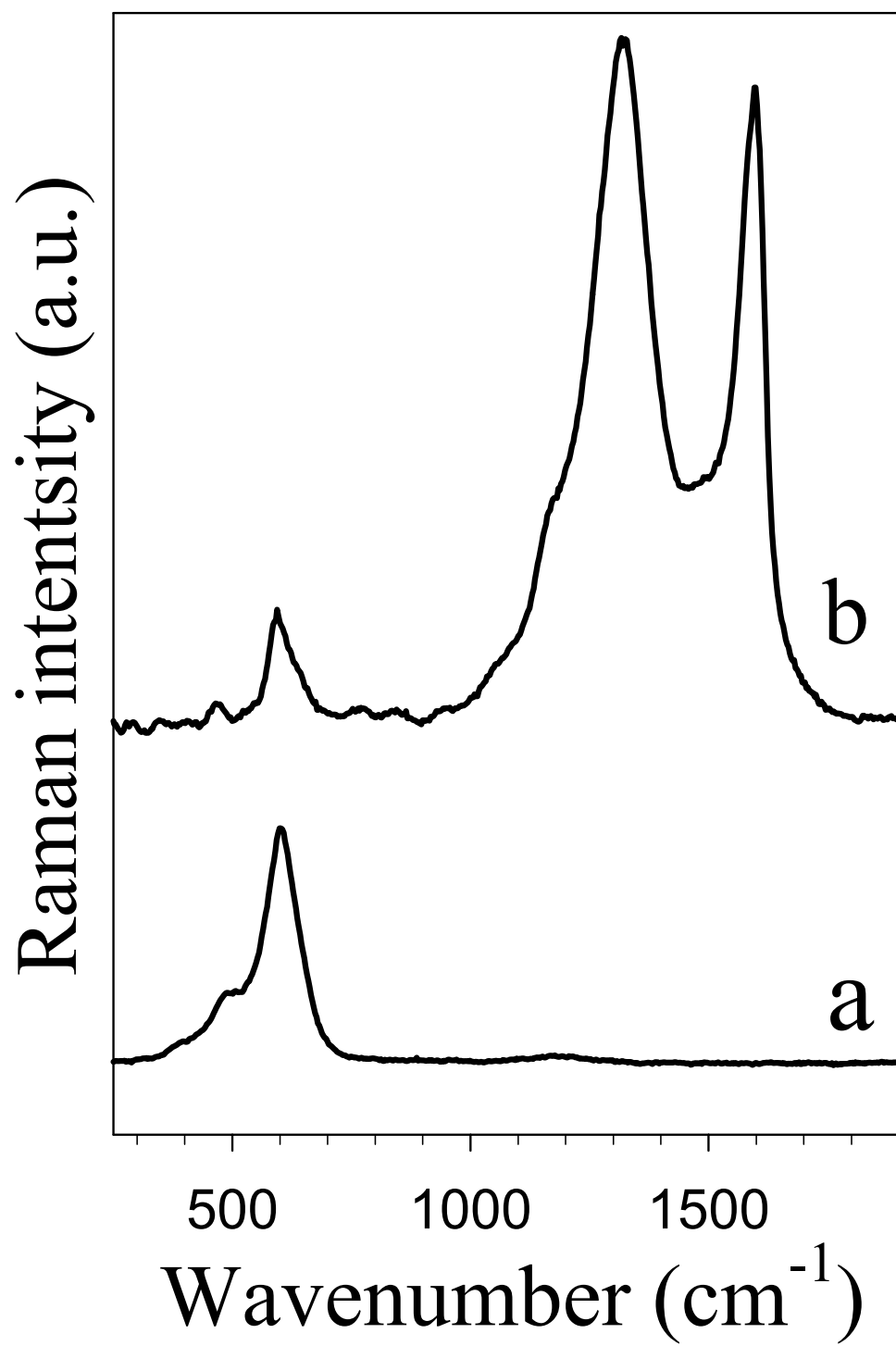
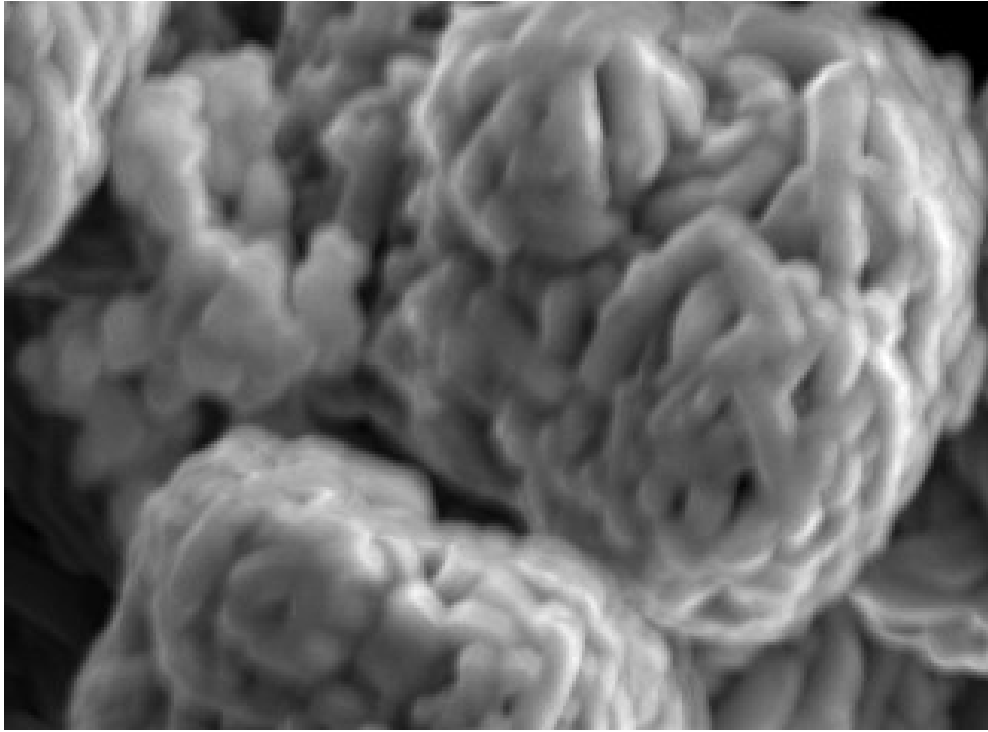


Figure 3

a



1 μm

b

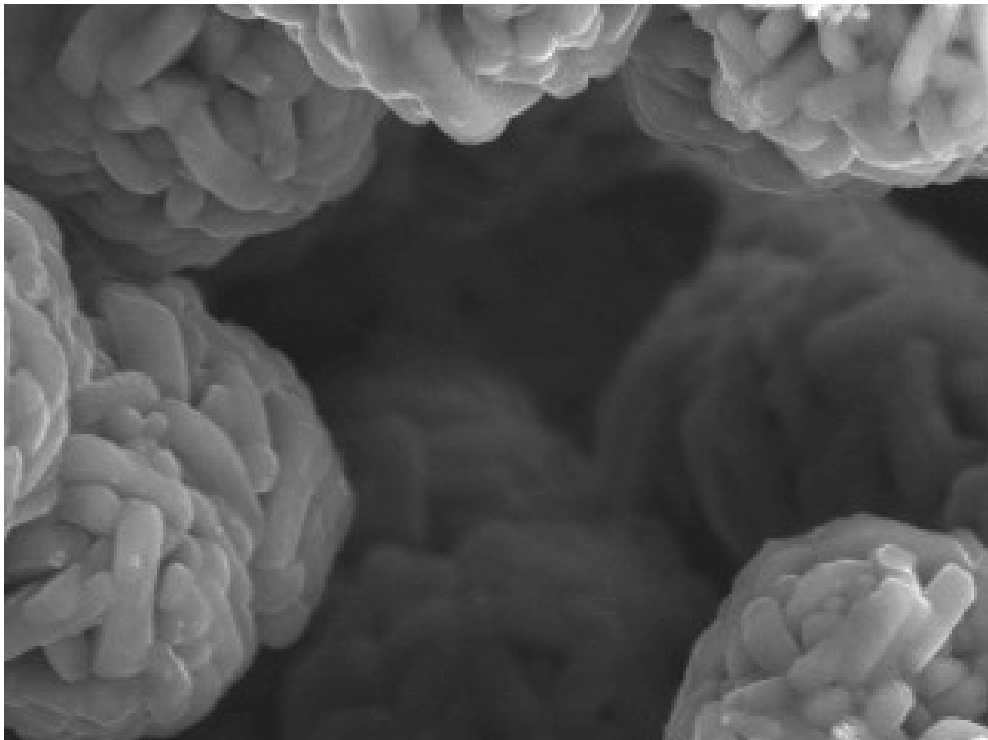


Figure 4

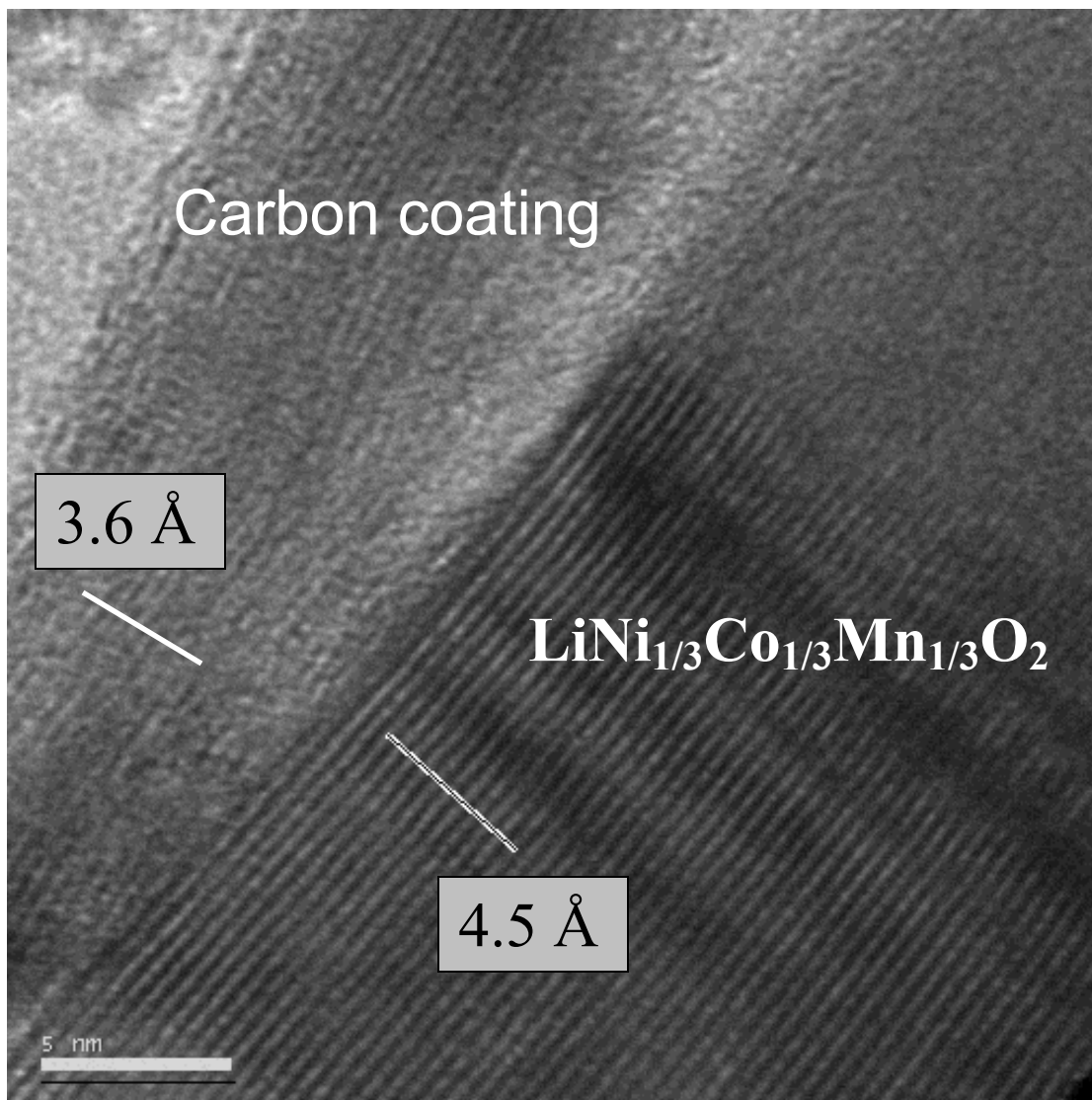


Figure 5

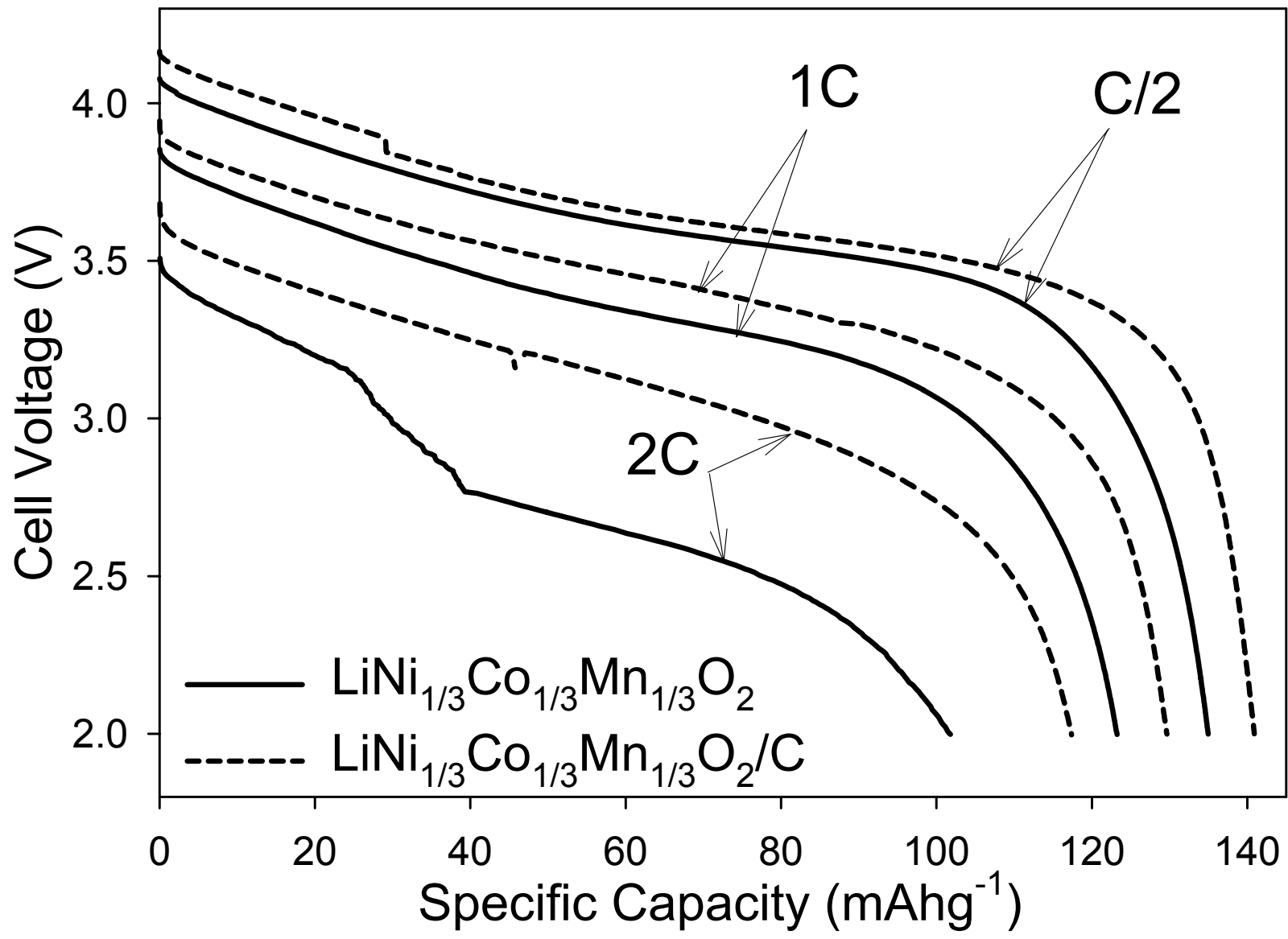


Figure 6

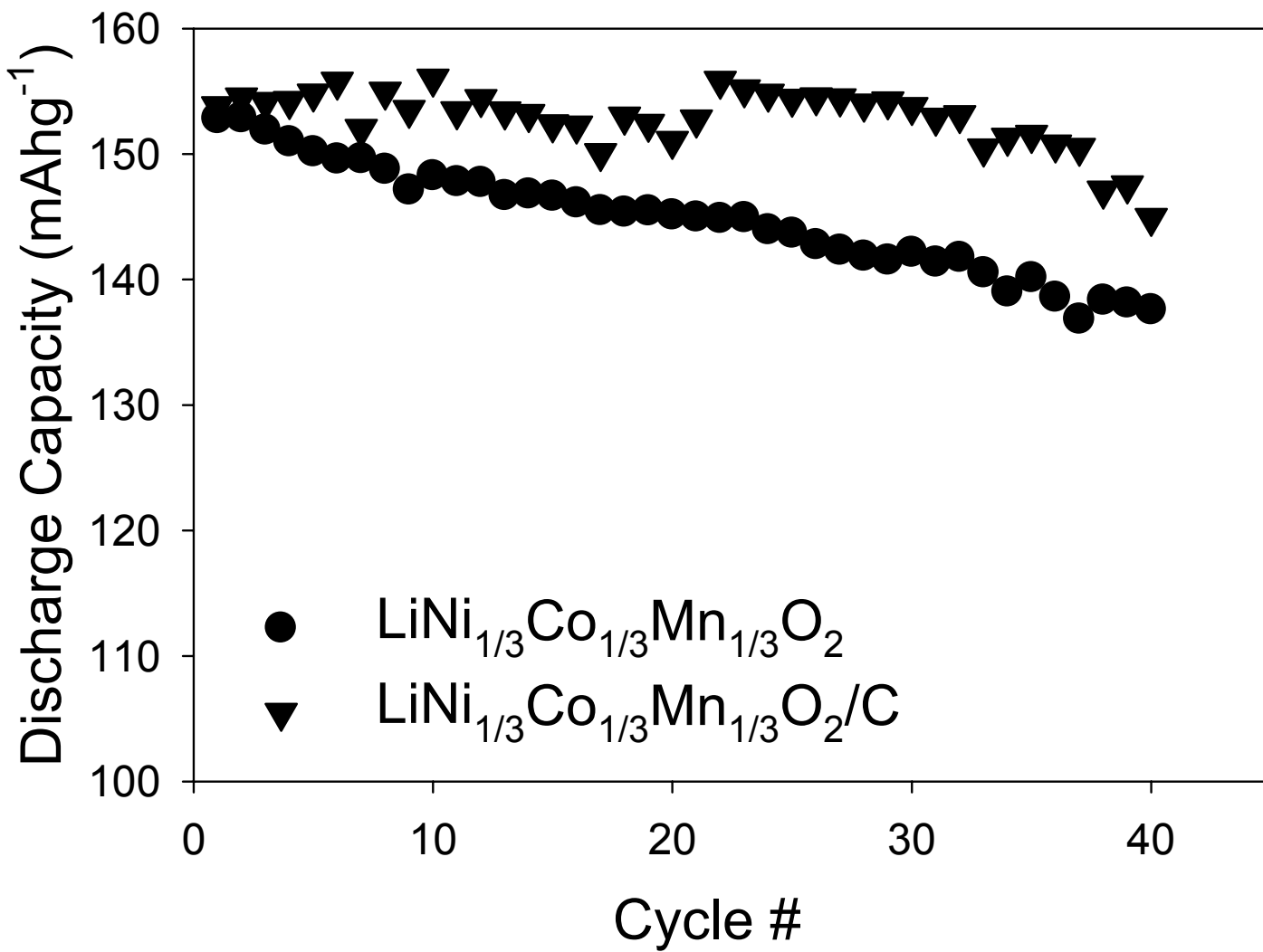


Figure 7

DISCLAIMER

This document was prepared as an account of work sponsored by the United States Government. While this document is believed to contain correct information, neither the United States Government nor any agency thereof, nor the Regents of the University of California, nor any of their employees, makes any warranty, express or implied, or assumes any legal responsibility for the accuracy, completeness, or usefulness of any information, apparatus, product, or process disclosed, or represents that its use would not infringe privately owned rights. Reference herein to any specific commercial product, process, or service by its trade name, trademark, manufacturer, or otherwise, does not necessarily constitute or imply its endorsement, recommendation, or favoring by the United States Government or any agency thereof, or the Regents of the University of California. The views and opinions of authors expressed herein do not necessarily state or reflect those of the United States Government or any agency thereof or the Regents of the University of California.